



Characterization of ^{18}F -fluorodeoxyglucose metabolic spatial distribution improves the differential diagnosis of indeterminate pulmonary nodules and masses with high fluorodeoxyglucose uptake

Jie Lin^{1#}, Ling Wang^{2#}, Xiaowei Ji¹, Xiangwu Zheng¹, Kun Tang¹

¹Department of PET/CT, The First Affiliated Hospital of Wenzhou Medical University, Wenzhou, China; ²Department of Nuclear Medicine, The First Affiliated Hospital of Wenzhou Medical University, Wenzhou, China

[#]These authors contributed equally to this work.

Correspondence to: Kun Tang, MD, PhD. The First Affiliated Hospital of Wenzhou Medical University, Xuefu North Road, Wenzhou 325000, China. Email: kuntang007@163.com.

Background: The aim of this study was to investigate the value of visual assessment of ^{18}F -fluorodeoxyglucose (^{18}F -FDG) metabolic spatial distribution (V-FMSD) in the diagnosis of indeterminate pulmonary nodules and masses with high ^{18}F -FDG uptake.

Methods: A total of 301 patients with indeterminate pulmonary nodules or masses who underwent ^{18}F -FDG positron emission tomography/computed tomography (PET/CT) imaging were retrospectively studied. The characteristics of ^{18}F -FDG metabolic spatial distribution (FMSD) in the proximal and distal regions of the lesions were visually analyzed using a 5-point scoring system. The sensitivity, specificity, accuracy, and area under receiver operating characteristic curve (AUC) were compared between V-FMSD and conventional PET/CT methods for the diagnosis of hypermetabolic indeterminate pulmonary nodules and masses.

Results: The V-FMSD results showed that 180 (92.8%) malignant lesions had a score of ≥ 3 and 78 (72.9%) benign lesions had a score of ≤ 2 . This indicated that the FMSD in the proximal region of malignant lesions was significantly higher than that of the distal region, and the FMSD in the proximal region of benign lesions was significantly lower than that of the distal region. V-FMSD had a specificity of 72.9%, which was markedly higher than those of the maximum standard uptake value (SUV_{max} ; 0%, $P < 0.001$) and the retention index (RI; 26.2%, $P < 0.001$). The AUC of V-FMSD was 0.886, which was significantly larger than those of the SUV_{max} (0.626, $P < 0.001$), RI (0.670, $P < 0.001$), and PET/CT (0.788, $P < 0.05$).

Conclusions: Our study found that pulmonary benign and malignant lesions have distinct FMSD characteristics. V-FMSD can therefore be used as a novel auxiliary marker to improve the diagnostic accuracy of hypermetabolic indeterminate pulmonary nodules and masses.

Keywords: ^{18}F -fluorodeoxyglucose (^{18}F -FDG); positron emission tomography; metabolic; cancer; lung nodules; maximum standard uptake value (SUV_{max})

Submitted Jun 17, 2020. Accepted for publication Nov 03, 2020.

doi: 10.21037/qims-20-768

View this article at: <http://dx.doi.org/10.21037/qims-20-768>

Introduction

With the increase in lung cancer screening and the growing global aging population, the incidence of lung cancer is increasing rapidly. Lung cancer has become the leading cause of cancer-associated death in the United States (1). Early detection strategies and surgical resection are the key to reducing lung cancer mortality (2).

Positron emission tomography/computed tomography (PET/CT), a noninvasive imaging technique, is widely used in the diagnosis and staging of pulmonary nodules (3,4). The maximum standard uptake value (SUV_{max}) is a key semiquantitative parameter for PET that measures the metabolic activity of a lesion. An SUV_{max} of 2.5 is usually used as the cut-off value for differentiating malignant from benign pulmonary lesions. However, ¹⁸F-fluorodeoxyglucose (¹⁸F-FDG) is not a tumor-specific agent; thus, intense FDG uptake can be observed in a significant percentage of benign pulmonary lesions, including inflammatory pseudotumors, cryptococcosis, and tuberculosis (5-7). Previous studies on the diagnosis of pulmonary lesions have reported high false positive rates associated with SUV (8,9). In particular, when the morphological characteristics of benign and malignant lesions are atypical, the false positive rate is higher. The high rates of false positive results have seen a corresponding increase in the rates of unnecessary invasive lung surgery and associated morbidity (10).

Therefore, a novel, alternative PET/CT-derived method is urgently needed to compensate for the high false positive rates resulting from the SUV method. In tumor development and progression, cancer cells migrate to and invade blood vessels (11); therefore, it can be speculated that cell metabolic activity will be higher in the proximal part of malignant tumors than in the distal part. Our previous findings have confirmed that the relative activity distribution (RAD) of ¹⁸F-FDG in malignant and benign solitary pulmonary nodules (SPNs) are markedly different. Furthermore, the use of SPN characterization with ¹⁸F-FDG RAD was much more specific than conventional SUV diagnostic methods in differentiating malignant from benign SPNs (12). However, the previous study only analyzed local metabolic distribution on small pulmonary nodules, and data needed to be obtained by performing complex diameter measurements and calculations. Therefore, the clinical feasibility of ¹⁸F-FDG metabolic spatial distribution (FMSD) in differentiating pulmonary nodules requires a wider range of samples and further simplification.

Therefore, the aim of the present study was to evaluate

whether visual assessment of ¹⁸F-FDG metabolic spatial distribution (V-FMSD), an easy-to-operate method, could improve the differential diagnosis of hypermetabolic pulmonary nodules and masses.

Methods

Patients

This retrospective study included 301 consecutive subjects (186 men and 115 women; mean age, 61.6 ± 11.2 years; range, 21–89 years) who underwent FDG PET/CT for suspected malignant pulmonary nodules or masses between January 1, 2015 and April 26, 2017. The exclusion criteria were as follows: (I) ¹⁸F-FDG SUV_{max} of the lesion < 2.5 ; (II) typical benign signs (central laminated or diffuse calcification, or popcorn pattern of calcification) or malignant signs (any three of the following: densely spiculated margin, vacuole sign, air bronchogram, vessel convergence, pleural indentation, and lesion with cavitation and wall thickness > 16 mm) detected by chest CT; (III) metastatic lesions or evidence of metastasis; (IV) multiple hypermetabolic nodules or masses in both lungs; (V) a previous history of lung biopsy or neoadjuvant chemoradiotherapy; (VI) a previous history of other cancer; (VII) obvious motion artifacts.

The pathological specimens were obtained by fiber optic bronchoscopy, percutaneous biopsy, resection by thoracotomy, or video-assisted thoracoscopic surgery after PET/CT examination. All malignant lesions were finally confirmed by pathology, and a definitive diagnosis of a benign lesion was made based on pathological analysis or at least 2 years of follow-up by chest CT. This study was approved by the Institutional Ethics Committee of the First Affiliated Hospital of Wenzhou Medical University, and written informed consent was obtained from all participants.

PET/CT acquisition

Patients fasted for at least 6 hours, and their serum glucose levels were < 110 mg/dL before intravenous injection of ¹⁸F-FDG (3.7 MBq/kg). Approximately 60 minutes after the injection, images were acquired using a hybrid PET/CT scanner (GEMINI TF 64, Philips, Best, Netherlands). The detailed PET/CT protocol can be found in our previous published study (13). The dual time point scans of the pulmonary lesions were performed 120 minutes after the injection. PET images were reconstructed using the

Table 1 The 5-point scoring system for the interpretation of the characteristics of FMSD

Scores	FDG uptake		Interpretation
	Proximal region	Distal region	
1	Significantly lower	Significantly higher	Definitely benign
2	Slightly lower	Slightly higher	Probably benign
3	Roughly homogeneous	Roughly homogeneous	Indeterminate
4	Slightly higher	Slightly lower	Probably malignant
5	Significantly higher	Significantly lower	Definitely malignant

FMSD, ^{18}F -FDG metabolic spatial distribution; FDG, fluorodeoxyglucose.

ordered subset expectation maximization (OSEM) method (33 subsets per iteration). All collected data were transferred onto the Philips Extend Brilliance Workstation (EBW, Philips, Best, Netherlands) 3.0 for reconstruction of PET, CT, and PET/CT fusion images.

Image analysis

Data measurement was independently performed by a nuclear medicine physician with 3 years of experience in PET/CT diagnosis. For each lesion, the SUV_{max} values of early and delayed scans were quantified. The retention index (RI) was calculated according to the following formula:

$$\text{RI} = \frac{100\% \times (\text{Dual time point } \text{SUV}_{\text{max}} - \text{Early } \text{SUV}_{\text{max}})}{\text{Early } \text{SUV}_{\text{max}}} [1]$$

In the assessment of SUV, the findings were considered positive when $\text{SUV}_{\text{max}} \geq 2.5$, and for delayed PET scans, $\text{RI} > 0$ was defined as positive.

The combined PET/CT images were independently assessed by two radiologists, each with over 30 years' experience in radiological diagnosis, who were blinded to the FMSD characteristics of the lesions. First, definitely positive findings were considered when ^{18}F -FDG uptake in lesions was significantly higher than that in the mediastinal blood pool. Second, for lesions with a slightly high uptake of ^{18}F -FDG, the morphological and metabolic lesion characteristics were combined to draw a comprehensive diagnosis. The diagnostic results were divided into probably positive or probably negative. When the findings were inconsistent between the two readers, a consensus was reached by discussion. Finally, definitely or possibly positive lesions were recorded as positive, and possibly negative lesions were recorded as negative.

The V-FMSD was analyzed by two nuclear medicine physicians each with 10 years of experience in PET/CT diagnosis, who were blinded to the information of the CT images and the final diagnoses of the patients. The proximal region of the lesion was defined as the area near the ipsilateral hilar, and the area far from the ipsilateral hilar was defined as the distal region (14). A 5-point scoring system was used to interpret the characteristics of FMSD, which represent the likelihood of the lesion being benign or malignant (Table 1, Figure 1). When the characteristics of FMSD in lesions were not obvious, the metabolic threshold could be manually adjusted on transverse PET images to assist the interpretation. When the interpretation scores were inconsistent between the two readers, a consensus was reached by discussion. Finally, a score of ≤ 2 was recorded as negative, while a score of ≥ 3 was recorded as positive.

Statistical analysis

Statistical analyses were performed with SPSS software, version 23.0 (IBM Corp., Armonk, New York, USA). The Mann-Whitney U-test was used to evaluate the continuous variables between malignant and benign lesions, and the results were described as mean \pm standard deviation. The Chi-squared test was performed to analyze the categorical data, and the results were presented as frequencies and percentages. Receiver operating characteristic (ROC) curve analysis was used to assess the performance of SUV_{max} , RI, combined PET/CT assessment, and V-FMSD for distinguishing malignant and benign lesions. The sensitivity, specificity, accuracy, positive predictive value (PPV), and negative predictive value (NPV) for each diagnostic method were also calculated. McNemar's test was used to compare the sensitivity, specificity, and accuracy of V-FMSD with those of the other methods. The intra-observer variability

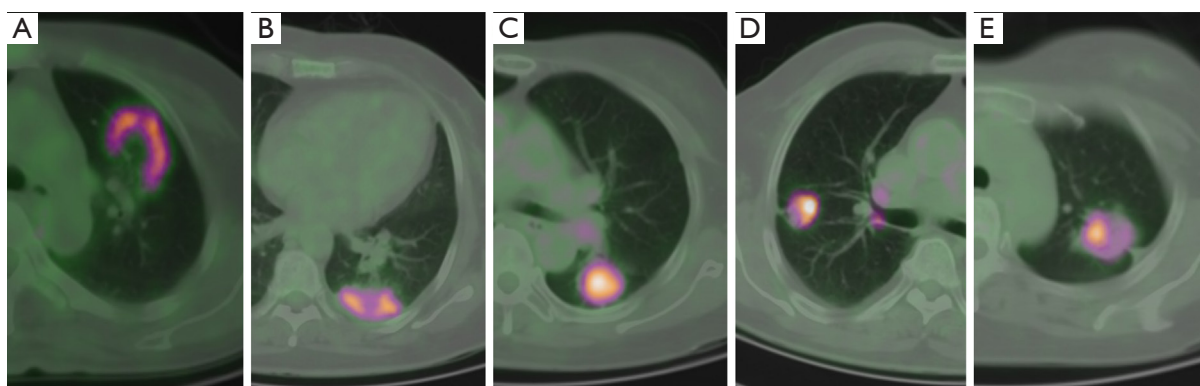


Figure 1 Representative FDG PET/CT images for the interpretation of the characteristics of FMSD. FDG PET/CT fused images demonstrate examples of lesions with FMSD grade 1–5, respectively. FDG, fluorodeoxyglucose; PET/CT, positron emission tomography/computed tomography; FMSD, ¹⁸F-FDG metabolic spatial distribution.

in visual scores was determined using Cohen's kappa coefficient (κ). A P value of <0.05 was considered to be statistically significant.

Results

General characteristic of subjects

Of 301 nodules and masses, 194 (64.5%) were malignant, and 107 (35.5%) were benign. The average maximum diameter of the lesions was 27.7 ± 13.2 mm (range, 8–63 mm). The malignant lesions were pathologically confirmed as adenocarcinoma (129, 66.5%), squamous cell carcinoma (41, 21.1%), adenosquamous carcinoma (13, 6.7%), small cell carcinoma (4, 2.1%), neuroendocrine carcinoma (4, 2.1%), and sarcomatoid carcinoma (3, 1.6%). The benign lesions, confirmed by pathology or follow-up, included tuberculosis (45, 42.1%), cryptococcal disease (18, 16.8%), chronic inflammation (12, 11.2%), hemangioma (9, 8.4%), focal organizing pneumonia (8, 7.5%), granulomatous inflammation (6, 5.6%), inflammatory pseudotumor (3, 2.8%), interstitial pneumonia (2, 1.9%), fungal infection (2, 1.9%), angiofollicular hyperplasia (1, 0.9%), and sclerotic silicotic nodule (1, 0.9%). The general characteristics of benign and malignant lesions are shown in *Table 2*. Compared with benign lesions, malignant tumors presented with significantly higher values for lesion size, SUV_{max} , delayed SUV_{max} , and RI.

The V-FMSD scoring results

The visual scoring results of FMSD in the benign and

malignant lesions are shown in *Table 3*. There were 180 (92.8%) malignant lesions with a score of ≥ 3 , which indicated that FDG metabolic distribution in the proximal region of the malignant lesions was significantly higher than that in the distal region (*Figure 2*). There were 78 (72.9%) benign lesions with a score of ≤ 2 , which indicated that FDG metabolic distribution in the proximal region of benign lesions was significantly lower than that in the distal region (*Figure 3*). The intra-observer variability in visual scores by the two observers is shown in *Table 4*. The Cohen's kappa coefficient demonstrated good agreement between the two observers' visual scores, with a kappa value of 0.635.

The diagnostic performance of different methods

The performance of V-FMSD for distinguishing malignant from benign lesions is shown in *Table 5*. When V-FMSD score ≥ 3 was used as the cut-off value, the sensitivity, specificity, PPV, NPV, and diagnostic accuracy of V-FMSD were 92.8%, 72.9%, 85.7%, 86.1%, and 89.2%, respectively. The diagnostic performance of V-FMSD showed no significant difference in distinguishing malignant and benign lesions in nodules of different sizes (all $P > 0.05$). Although the sensitivity of V-FMSD did not differ significantly from those of the other three methods (all $P > 0.05$), its specificity (72.9%) was significantly higher than those of SUV_{max} (0%, $P < 0.001$) and RI (26.2%, $P < 0.001$) (*Table 6*).

The ROC curves for the different methods in the diagnosis of malignant and benign lesions are shown in *Figure 4*. The areas under the ROC curves (AUCs) of

Table 2 General characteristics of subjects

Characteristics	Overall (n=301)	Benign (n=107)	Malignant (n=194)	P value
Age, years	61.6±11.2	57.6±12.6	63.9±9.6	<0.001
Sex, n (%)				0.014
Male	186 (61.8)	76 (71.0)	110 (56.7)	
Female	115 (38.2)	31 (29.0)	84 (43.3)	
Tumor site, n (%)				0.128
RUL	99 (32.9)	42 (39.3)	57 (29.4)	
RML	20 (6.6)	6 (5.6)	14 (7.2)	
RLL	75 (24.9)	26 (24.3)	49 (25.3)	
LUL	67 (22.3)	16 (15.0)	51 (26.3)	
LLL	40 (13.3)	17 (15.9)	23 (11.9)	
Tumor size, mm	27.7±13.2	24.2±13.4	29.6±12.8	0.001
FBG, mg/dl	5.6±1.2	5.6±1.5	5.5±1.1	0.574
SUV _{max}	6.7±3.9	5.7±3.4	7.3±4.0	<0.001
Delayed SUV _{max}	7.9±5.0	6.0±3.6	8.6±5.3	0.001
RI (%)	26.1±21.8	16.8±21.6	29.8±20.9	0.001

RUL, right upper lobe; RML, right middle lobe; RLL, right lower lobe; LUL, left upper lobe; LLL, left lower lobe; FBG, fasting blood glucose; SUV_{max}, maximum standard uptake value; RI, retention index.

Table 3 Scoring results of V-FMSD in benign and malignant lesions

	Scoring					Total
	1	2	3	4	5	
Benign lesions, n	15	63	20	7	2	107
Malignant lesions, n	0	14	51	92	37	194

V-FMSD, visual assessment of ¹⁸F-fluorodeoxyglucose (¹⁸F-FDG) metabolic spatial distribution.

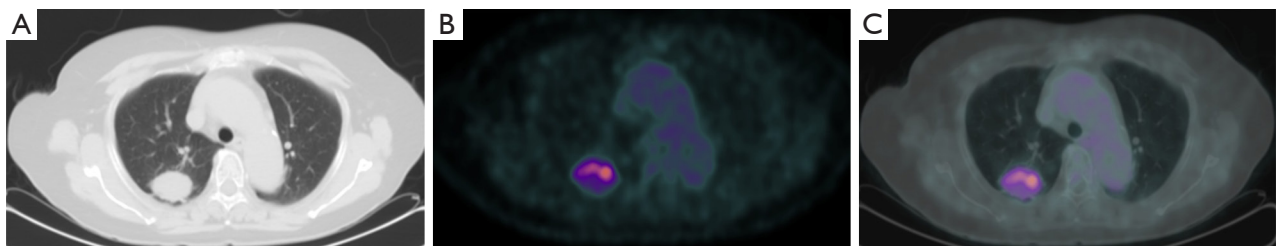


Figure 2 Images from a 65-year-old female patient with adenocarcinoma. Transaxial CT (A) showed a nodule in the right upper lobe. The nodule presented profound FDG uptake with an SUV_{max} of 6.4 on transaxial PET (B) and fused (C) images. The FMSD in the proximal region of the nodule was significantly higher than that in the distal region, and the V-FMSD score was 5, which indicated a malignant lesion. CT, computed tomography; FDG, fluorodeoxyglucose; SUV_{max}, maximum standard uptake value; PET, positron emission tomography; FMSD, ¹⁸F-FDG metabolic spatial distribution; V-FMSD, visual assessment of ¹⁸F-FDG metabolic spatial distribution.



Figure 3 Images from a 49-year-old female patient with tuberculosis. Transaxial CT (A) showed a mass in the right lower lobe. The lesion displayed profound FDG uptake with a SUV_{max} of 8.4 on transaxial PET (B) and fused (C) images. The FMSD in the proximal region of lesion was significantly lower than that in the distal region, and the V-FMSD score was 1, which indicated a benign lesion. CT, computed tomography; FDG, fluorodeoxyglucose; SUV_{max} , maximum standard uptake value; PET, positron emission tomography; FMSD, ¹⁸F-FDG metabolic spatial distribution; V-FMSD, visual assessment of ¹⁸F-FDG metabolic spatial distribution.

Table 4 Assessment of intra-observer variability in visual scores

Observer 2	Observer 1					Overall
	1	2	3	4	5	
1	14	5	1	0	0	20
2	5	53	14	4	0	76
3	0	3	44	10	1	58
4	0	3	12	62	8	85
5	0	1	6	12	43	62
Overall	14	65	81	97	44	301

Kappa value 0.635.

Table 5 The performance of V-FMSD for distinguishing benign and malignant lesions

Groups	Sensitivity	Specificity	TP	TN	FP	FN	PPV	NPV	Accuracy
Overall, n=301	92.8	72.9	180	78	29	14	86.1	89.2	85.7
<10 mm, n=3	–	–	1	1	1	0	–	–	–
10–19 mm, n=80	91.2	76.1	31	35	11	3	73.8	92.1	82.5
20–29 mm, n=106	93.5	75.9	72	22	7	5	91.1	81.5	88.7
30–49 mm, n=89	92.3	66.7	60	16	8	5	88.2	69.6	85.4
≥50 mm, n=23	94.1	66.6	16	4	2	1	88.9	80.0	87.0

V-FMSD, visual assessment of ¹⁸F-fluorodeoxyglucose (¹⁸F-FDG) metabolic spatial distribution; TP, true positive; TN, true negative; FP, false positive; FN, false negative; PPV, positive predictive value; NPV, negative predictive value.

Table 6 Comparison of diagnostic value among the different methods

	Sensitivity	Specificity	TP	TN	FP	FN	PPV	NPV	Accuracy
SUV _{max} ≥2.5	100	0	194	0	107	0	64.5	0	64.5
Dual time point RI (%) >0	95.3	26.2	185	28	79	9	71.2	78.0	70.8
Visual PET/CT assessment	95.9	61.7	186	66	41	8	81.9	83.7	83.7
V-FMSD score ≥3	92.8	72.9*	180	78	29	14	86.1	89.2	85.7

*, Significant difference (P<0.001) between specificity of visual score and specificity of SUV_{max} and dual time point RI. SUV_{max}, maximum standard uptake value; RI, retention index; V-FMSD, visual assessment of ¹⁸F-FDG metabolic spatial distribution; TP, true positive; TN, true negative; FP, false positive; FN, false negative; PPV, positive predictive value; NPV, negative predictive value.

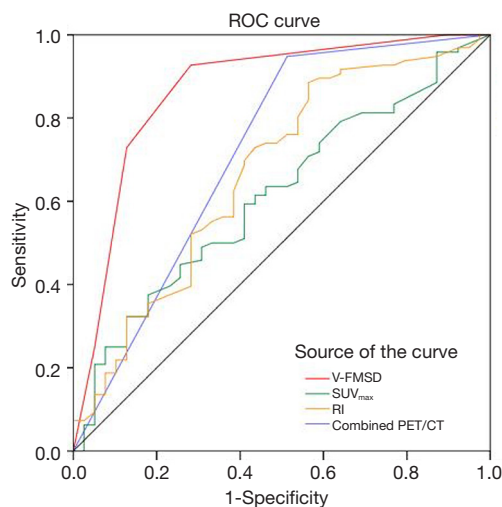


Figure 4 The ROC curves plotted for the different diagnostic methods. ROC, receiver operating characteristic.

SUV_{max}, RI, combined PET/CT assessment, and V-FMSD were 0.626, 0.670, 0.788, and 0.886, respectively. The AUC of V-FMSD was significantly larger than those of SUV_{max}, RI, and combined PET/CT (all P<0.05) (Table 7).

Discussion

The present study firstly evaluated the performance of V-FMSD for distinguishing pulmonary malignant and benign lesions. The results indicated that FDG uptake in the proximal region of malignant lesions was significantly higher than that in the distal region, and the FMSD of benign lesions was opposite to that of malignant lesions. Furthermore, FMSD demonstrated higher diagnostic efficacy than SUV_{max} and RI in the diagnosis of pulmonary hypermetabolic lesions, especially in terms of specificity. Therefore, this method should be considered as a valuable investigative addition in the assessment of indeterminate

Table 7 Comparison of AUCs among the different methods

Variable(s)	Area	Std. Error	Significance	95% CI		Z value	P value
				Lower	Lower		
V-FMSD	0.886	0.021	0.000	0.845	0.928		
SUVmax	0.626	0.033	0.000	0.561	0.691	6.646 ^a	<0.001
Dual time point RI	0.670	0.033	0.000	0.605	0.735	5.521 ^b	<0.001
Visual PET/CT assessment	0.788	0.031	0.000	0.727	0.848	2.615 ^c	0.004

^a, V-FMSD vs. SUV_{max}; ^b, V-FMSD vs. RI; ^c, V-FMSD vs. visual PET/CT. AUC, area under the ROC curves; V-FMSD, visual assessment of ¹⁸F-FDG metabolic spatial distribution; SUV_{max}, maximum standard uptake value; RI, retention index; PET/CT, positron emission tomography/computed tomography.

pulmonary lesions.

¹⁸F-FDG PET/CT is a well-established imaging modality for the diagnosis of patients with suspected lung cancer. However, the overlap of SUV_{max} between benign and malignant pulmonary lesions limits PET/CT diagnostic value. Previous studies have reported the specificity of PET for the diagnosis of malignant pulmonary nodules to vary between 13% and 89% (15-19). Inflammatory lesions have been shown to account for 73% of benign non-neoplastic lesions with increased ¹⁸F-FDG uptake (20). The ¹⁸F-FDG uptake which represents the levels of cellular glucose metabolism in inflammatory and oncological diseases shares the similar mechanism and is mediated by the glucose transporters GLUT1-5 (21,22). In active inflammation and granulomatous diseases, such as tuberculosis and sarcoidosis, increased ¹⁸F-FDG accumulation appears in cells due to the expression of glucose transporters, especially GLUT1 in activated leukocytes, macrophages, and T lymphocytes (23-25).

Since the prevalence of tuberculosis in China is higher than in Western countries, the accuracy of ¹⁸F-FDG PET/CT for the identification of pulmonary abnormalities may be decreased. In the present study, almost half (42.1%) of benign lesions were tuberculosis, and the average SUV_{max} of those tubercular lesions was 6.7. All of the cases included in this study had hypermetabolic lesions with an SUV_{max} >2.5. When SUV_{max} 2.5 was used as the cut-off value to diagnose lung cancer, the number of false positive cases was 107, and the specificity and accuracy were 0% and 64.5%, respectively. This showed that the value of SUV_{max} in the diagnosis of hypermetabolic lung nodules and masses was extremely limited. PET/CT combines lesion morphology and metabolic information. However, for hypermetabolic pulmonary nodules and masses with atypical CT morphology, the diagnostic basis is more dependent on the metabolic information of the lesion. In this study, the number of false positive cases with PET/CT combined analysis was 41, of which tuberculosis and cryptococcal bacteria accounted for a large proportion. Therefore, to further improve diagnostic accuracy for hypermetabolic nodules and masses, it is necessary to explore novel auxiliary analysis methods.

Our previous study confirmed the difference in RAD of ¹⁸F-FDG between malignant and benign SPNs (12). To further simplify the evaluation, the present study used the hilar as a reference for the division of lesions into proximal and distal regions, and visually interpreted the spatial distribution of ¹⁸F-FDG uptake in these two regions of benign and malignant lesions. The results of this study

showed that in the malignant lesions, the ¹⁸F-FDG uptake in the proximal region was significantly higher than that of the distal region. In benign lesions, the spatial distribution of ¹⁸F-FDG was opposite to that in malignant lesions, with the ¹⁸F-FDG uptake lower in the proximal region than in the distal region. In regard to the pathological mechanisms underlying the metabolic spatial heterogeneity between benign and malignant lesions, one of the possible reasons may be related to angiogenesis and its distribution. Recent studies have indicated that angiogenesis plays an important role in tumor formation, growth, metastasis, and recurrence (26,27). Abnormal tumor vasculature may lead to altered perfusion, which is believed to be the major extrinsic driver of metabolism through its effects on oxygen and substrate delivery (28). Also, the main blood supply for lung tumors comes from the bronchial artery, while inflammation is more likely to stimulate the extrapulmonary circulation artery to participate in blood supply. Therefore, the blood supply in the proximal region of lung tumors is more abundant, and the same phenomenon can be observed in the distal region of lung inflammation. However, the metabolic distribution in a lesion is influenced by many factors, including the tumor microenvironment, genetic heterogeneity, and immune factors (29-31).

The hallmarks of the V-FMSD method are its simplicity and easy operability in clinic. Furthermore, this simple visual analysis can achieve a high diagnostic performance. Although the sensitivity of V-FMSD was similar to those of the PET/CT conventional markers, the specificity of this new method was significantly higher than those of SUV_{max} and RI. However, the visual difference in metabolic distribution in small nodules was not obvious due to their small volume, especially for nodules <10 mm in size. However, the diagnostic performance of V-FMSD for nodules of different sizes (>10 mm) showed no statistical significance in distinguishing between malignant and benign lesions. The pathologies of the 14 malignant nodules with FMSD grade 2 were adenocarcinoma (9, 64.3%), squamous cell carcinoma (2, 14.3%), adenosquamous carcinoma (2, 14.3%), and small cell carcinoma (1, 7.1%), respectively. Of the 29 cases of benign nodules with FMSD grade 3-5, almost half were tuberculosis (13, 44.8%). Compared with the findings of previous studies, our results still showed the conventional PET/CT markers to have lower sensitivity and specificity (3,32,33). The major reason for this might be the high proportion of benign hypermetabolic lesions included in this study. However, this novel visual assessment can still improve the diagnostic performance when the

CT morphology is atypical. Therefore, V-FMSD can be considered a novel routine auxiliary diagnostic method for the diagnosis of indeterminate pulmonary nodules and masses with high ^{18}F -FDG uptake.

The main limitation of this study is that visual analysis is a subjective empirical judgment which may introduce subjective bias. In the present study, the Kappa value for intra-observer agreement was 0.635, which suggested that consistency could be further improved. In clinical practice, multiple comparative analysis of FMSD by adjusting the SUV threshold can be used to improve the repeatability of the assessment. In patient selection, we only included pulmonary nodules and masses with avid ^{18}F -FDG uptake, which might have introduced selection bias. Moreover, this study did not explore the related molecular mechanisms. However, our pre-experiments showed that the expression levels of CD31 and epidermal growth factor receptor (EGFR) were different between the proximal and distal regions of benign and malignant lung lesions, which suggested that the difference in FMSD may be correlated with tumor angiogenesis and its distribution. Therefore, future studies will explore the possible related mechanisms.

Conclusions

In summary, we found that pulmonary benign and malignant lesions had distinct FMSD characteristics. FDG uptake in the proximal region of malignant lesions was significantly higher than that in the distal region, and the FMSD of benign lesions was opposite to that of malignant lesions. V-FMSD is a simple and easy procedure; therefore, it can be used as a novel auxiliary marker in clinical practice to improve the diagnostic accuracy for indeterminate pulmonary nodules and masses with avid ^{18}F -FDG uptake.

Acknowledgments

Funding: This work was supported by Zhejiang Province Public Welfare Technology Application Research Project (No. LGF19H180012) and Wenzhou Science and Technology Program (No. Y20170833).

Footnote

Conflicts of Interest: All authors have completed the ICMJE uniform disclosure form (available at <http://dx.doi.org/10.21037/qims-20-768>). The authors have no conflicts

of interest to declare.

Ethical Statement: This study was approved by the Institutional Ethics Committee of the First Affiliated Hospital of Wenzhou Medical University. Written informed consent was obtained from all patients.

Open Access Statement: This is an Open Access article distributed in accordance with the Creative Commons Attribution-NonCommercial-NoDerivs 4.0 International License (CC BY-NC-ND 4.0), which permits the non-commercial replication and distribution of the article with the strict proviso that no changes or edits are made and the original work is properly cited (including links to both the formal publication through the relevant DOI and the license). See: <https://creativecommons.org/licenses/by-nc-nd/4.0/>.

References

1. Siegel R, Naishadham D, Jemal A. Cancer statistics, 2012. *CA Cancer J Clin* 2012;62:10-29.
2. Patz EF, Jr., Rossi S, Harpole DH, Jr., Herndon JE, Goodman PC. Correlation of tumor size and survival in patients with stage IA non-small cell lung cancer. *Chest* 2000;117:1568-71.
3. Garcia-Velloso MJ, Bastarrika G, de-Torres JP, Lozano MD, Sanchez-Salcedo P, Sancho L, Nunez-Cordoba JM, Campo A, Alcaide AB, Torre W, Richter JA, Zulueta JJ. Assessment of indeterminate pulmonary nodules detected in lung cancer screening: Diagnostic accuracy of FDG PET/CT. *Lung cancer (Amsterdam, Netherlands)* 2016;97:81-6.
4. Zhang Y, Ni J, Wei K, Tian J, Sun S. CT, MRI, and F-18 FDG PET for the detection of non-small-cell lung cancer (NSCLC): A protocol for a network meta-analysis of diagnostic test accuracy. *Medicine (Baltimore)* 2018;97:e12387.
5. Sánchez-Montalvá A, Barrios M, Salvador F, Villar A, Tórtola T, Molina-Morant D, Lorenzo-Bosquet C, Espinosa-Pereiro J, Molina I. Usefulness of FDG PET/CT in the management of tuberculosis. *PLoS One* 2019;14:e0221516.
6. Chang JM, Lee HJ, Goo JM, Lee HY, Lee JJ, Chung JK, Im JG. False positive and false negative FDG-PET scans in various thoracic diseases. *Korean J Radiol* 2006;7:57-69.
7. Yu WY, Lu PX, Assadi M, Huang XL, Skrahin A, Rosenthal A, Gabrielian A, Tartakovsky M, Wang YXJ. Updates on (18)F-FDG-PET/CT as a clinical tool for

- tuberculosis evaluation and therapeutic monitoring. *Quant Imaging Med Surg* 2019;9:1132-46.
8. Feng M, Yang X, Ma Q, He Y. Retrospective analysis for the false positive diagnosis of PET-CT scan in lung cancer patients. *Medicine (Baltimore)* 2017;96:e7415.
 9. Maiga AW, Deppen SA, Mercaldo SF, Blume JD, Montgomery C, Vaszar LT, Williamson C, Isbell JM, Rickman OB, Pinkerman R, Lambright ES, Nesbitt JC, Grogan EL. Assessment of Fluorodeoxyglucose F18-Labeled Positron Emission Tomography for Diagnosis of High-Risk Lung Nodules. *JAMA Surg* 2018;153:329-34.
 10. Grogan EL, Deppen SA, Ballman KV, Andrade GM, Verdial FC, Aldrich MC, Chen CL, Decker PA, Harpole DH, Cerfolio RJ, Keenan RJ, Jones DR, D'Amico TA, Shrager JB, Meyers BF, Putnam JB, Jr. Accuracy of fluorodeoxyglucose-positron emission tomography within the clinical practice of the American College of Surgeons Oncology Group Z4031 trial to diagnose clinical stage I non-small cell lung cancer. *Ann Thorac Surg* 2014;97:1142-8.
 11. Wu PH, Giri A, Sun SX, Wirtz D. Three-dimensional cell migration does not follow a random walk. *Proc Natl Acad Sci U S A* 2014;111:3949-54.
 12. Zhao L, Tong L, Lin J, Tang K, Zheng S, Li W, Cheng D, Yin W, Zheng X. Characterization of solitary pulmonary nodules with 18F-FDG PET/CT relative activity distribution analysis. *Eur Radiol* 2015;25:1837-44.
 13. Xu M, Wang L, Ouyang M, Lin J, Wang L, Zheng X, Miao S, Tang K. Prediction of lymph node metastasis by PET/CT metabolic parameters in patients with esophageal squamous cell carcinoma. *Nucl Med Commun* 2019;40:933-9.
 14. Wu L, Cao G, Zhao L, Tang K, Lin J, Miao S, Lin T, Sun J, Zheng X. Spectral CT Analysis of Solitary Pulmonary Nodules for Differentiating Malignancy from Benignancy: The Value of Iodine Concentration Spatial Distribution Difference. *Biomed Res Int* 2018;2018:4830659.
 15. van Gómez López O, García Vicente AM, Honguero Martínez AF, Jiménez Londoño GA, Vega Caicedo CH, León Atance P, Soriano Castrejón ÁM. (18)F-FDG-PET/CT in the assessment of pulmonary solitary nodules: comparison of different analysis methods and risk variables in the prediction of malignancy. *Transl Lung Cancer Res* 2015;4:228-35.
 16. Li Y, Su M, Li F, Kuang A, Tian R. The value of (1)(8) F-FDG-PET/CT in the differential diagnosis of solitary pulmonary nodules in areas with a high incidence of tuberculosis. *Ann Nucl Med* 2011;25:804-11.
 17. Hashimoto Y, Tsujikawa T, Kondo C, Maki M, Momose M, Nagai A, Ohnuki T, Nishikawa T, Kusakabe K. Accuracy of PET for diagnosis of solid pulmonary lesions with 18F-FDG uptake below the standardized uptake value of 2.5. *J Nucl Med* 2006;47:426-31.
 18. Taralli S, Scolozzi V, Foti M, Ricciardi S, Forcione AR, Cardillo G, Calcagni ML. (18)F-FDG PET/CT diagnostic performance in solitary and multiple pulmonary nodules detected in patients with previous cancer history: reports of 182 nodules. *Eur J Nucl Med Mol Imaging* 2019;46:429-36.
 19. Matthies A, Hickeson M, Cuchiara A, Alavi A. Dual time point 18F-FDG PET for the evaluation of pulmonary nodules. *J Nucl Med* 2002;43:871-5.
 20. Metser U, Even-Sapir E. Increased (18) F-fluorodeoxyglucose uptake in benign, nonphysiologic lesions found on whole-body positron emission tomography/computed tomography (PET/CT): accumulated data from four years of experience with PET/CT. *Semin Nucl Med* 2007;37:206-22.
 21. Brown RS, Leung JY, Kison PV, Zasadny KR, Flint A, Wahl RL. Glucose transporters and FDG uptake in untreated primary human non-small cell lung cancer. *J Nucl Med* 1999;40:556-65.
 22. Rivlin M, Navon G. Molecular imaging of tumors by chemical exchange saturation transfer MRI of glucose analogs. *Quant Imaging Med Surg* 2019;9:1731-46.
 23. Huber H, Hodolic M, Stelzmüller I, Wunn R, Hatzl M, Fellner F, Lamprecht B, Rubello D, Colletti PM, Gabriel M. Malignant disease as an incidental finding at F-18-FDG-PET/CT scanning in patients with granulomatous lung disease. *Nucl Med Commun* 2015;36:430-7.
 24. Mochizuki T, Tsukamoto E, Kuge Y, Kanegae K, Zhao S, Hikosaka K, Hosokawa M, Kohanawa M, Tamaki N. FDG uptake and glucose transporter subtype expressions in experimental tumor and inflammation models. *J Nucl Med* 2001;42:1551-5.
 25. Keijsers RG, van den Heuvel DA, Grutters JC. Imaging the inflammatory activity of sarcoidosis. *Eur Respir J* 2013;41:743-51.
 26. Herbst RS, Onn A, Sandler A. Angiogenesis and lung cancer: prognostic and therapeutic implications. *J Clin Oncol* 2005;23:3243-56.
 27. Folkman J. Angiogenesis in cancer, vascular, rheumatoid and other disease. *Nat Med* 1995;1:27-31.
 28. Guillaumond F, Leca J, Olivares O, Lavaut MN, Vidal N, Berthezene P, Dusetti NJ, Loncle C, Calvo E, Turrini O, Iovanna JL, Tomasini R, Vasseur S. Strengthened

- glycolysis under hypoxia supports tumor symbiosis and hexosamine biosynthesis in pancreatic adenocarcinoma. *Proc Natl Acad Sci U S A* 2013;110:3919-24.
29. Navin N, Kendall J, Troge J, Andrews P, Rodgers L, McIndoo J, Cook K, Stepansky A, Levy D, Esposito D, Muthuswamy L, Krasnitz A, McCombie WR, Hicks J, Wigler M. Tumour evolution inferred by single-cell sequencing. *Nature* 2011;472:90-4.
 30. Hensley CT, Faubert B, Yuan Q, Lev-Cohain N, Jin E, Kim J, Jiang L, Ko B, Skelton R, Loudat L, Wozzak M, Klimko C, McMillan E, Butt Y, Ni M, Oliver D, Torrealba J, Malloy CR, Kernstine K, Lenkinski RE, DeBerardinis RJ. Metabolic Heterogeneity in Human Lung Tumors. *Cell* 2016;164:681-94.
 31. Wang L, Zhu B, Zhang M, Wang X. Roles of immune microenvironment heterogeneity in therapy-associated biomarkers in lung cancer. *Semin Cell Dev Biol* 2017;64:90-7.
 32. Gould MK, Maclean CC, Kuschner WG, Rydzak CE, Owens DK. Accuracy of positron emission tomography for diagnosis of pulmonary nodules and mass lesions: a meta-analysis. *JAMA* 2001;285:914-24.
 33. Graeber GM, Gupta NC, Murray GF. Positron emission tomographic imaging with fluorodeoxyglucose is efficacious in evaluating malignant pulmonary disease. *J Thorac Cardiovasc Surg* 1999;117:719-27.

Cite this article as: Lin J, Wang L, Ji X, Zheng X, Tang K. Characterization of ¹⁸F-fluorodeoxyglucose metabolic spatial distribution improves the differential diagnosis of indeterminate pulmonary nodules and masses with high fluorodeoxyglucose uptake. *Quant Imaging Med Surg* 2021;11(4):1543-1553. doi: 10.21037/qims-20-768